Influences of the ocean surface mixed layer and thermohaline stratification on Arctic Sea ice in the central Canada Basin

J. M. Toole,[1] M.-L. Timmermans,[2] D. K. Perovich,[3] R. A. Krishfield,[1] A. Proshutinsky,[1] and J. A. Richter-Menge[3]

[1]   Variations in the Arctic central Canada Basin mixed layer properties are documented based on a subset of nearly 6500 temperature and salinity profiles acquired by Ice-Tethered Profilers during the period summer 2004 to summer 2009 and analyzed in conjunction with sea ice observations from ice mass balance buoys and atmosphere-ocean heat flux estimates. The July–August mean mixed layer depth based on the Ice-Tethered Profiler data averaged 16 m (an overestimate due to the Ice-Tethered Profiler sampling characteristics and present analysis procedures), while the average winter mixed layer depth was only 24 m, with individual observations rarely exceeding 40 m. Guidance interpreting the observations is provided by a 1-D ocean mixed layer model. The analysis focuses attention on the very strong density stratification at the base of the mixed layer in the Canada Basin that greatly impedes surface layer deepening and thus limits the flux of deep ocean heat to the surface that could influence sea ice growth/ decay. The observations additionally suggest that efficient lateral mixed layer restratification processes are active in the Arctic, also impeding mixed layer deepening.

Citation: Toole, J. M., M.-L. Timmermans, D. K. Perovich, R. A. Krishfield, A. Proshutinsky, and J. A. Richter-Menge (2010), Influences of the ocean surface mixed layer and thermohaline stratification on Arctic Sea ice in the central Canada Basin, *J. Geophys. Res.*, *115*, C10018, doi:10.1029/2009JC005660.

1.   Introduction

[2]   The Arctic Ocean's surface mixed layer (ML) constitutes the dynamical and thermodynamical link between the sea ice and the underlying waters. Wind stress, acting directly on the ML or via wind-forced ice motion, produces ML currents that in turn drive deep ocean flows. Shear between the surface and underlying layer can support ML deepening (shear mixing) as can a surface buoyancy sink (convection), while restratification due to a surface buoyancy source or lateral eddy processes can manifest as ML shoaling. Departure of ML temperature from the local freezing point is intimately related to basal sea ice growth and melting. In turn, ML temperature is strongly governed by the divergence of the heat fluxes into the mixed layer across its upper and lower interfaces: the former via air-sea exchange at leads and conduction and radiation through the ice (and melt water runoff), the latter via turbulent mixing and entrainment at the layer base. Here variations in central Canada Basin ML properties are documented based on nearly 6500 temperature and salinity profiles acquired by Ice-Tethered Profilers (ITP) [*Krishfield et al.*, 2008a] during

the period summer 2004 to summer 2009 and analyzed in conjunction with sea ice observations from ice mass balance buoys (IMB) [*Richter-Menge et al.*, 2006] and atmosphere-ocean heat flux estimates. The aim of the present work is to quantify the central Canada Basin ML characteristics in the 2004–2009 period and investigate the relationships between the sea ice, ML, and upper-ocean stratification.

[3]   The ITP data reveal that the central Canada Basin is presently characterized by low salinity (average ~28), thin surface mixed layers. Observed ML depths were commonly <12 m in summer and very rarely exceeded 40 m in winter. In the following, we demonstrate using a simple 1-D model that the large vertical density gradient due to these low surface salinities in combination with rather small energy input to surface ageostrophic motions account for these thin MLs. It is subsequently argued that subsurface (below ~45 m depth) ocean heat reservoirs, in particular, the intrusions of Pacific Summer Water that are found in the central Canada Basin, presently exert little influence on the seasonal evolution of the sea ice in this region. These conclusions largely echo the findings of *Maykut and McPhee* [1995], who analyzed Canada Basin observations acquired from manned drifting ice camps in 1975–1976. The present study also builds on the more recent work of *Shaw et al.* [2009] that was based on data from the SHEBA (Surface Heat Budget of the Arctic) expedition: another Canada Basin manned ice camp program and relates to the *Shimada et al.* [2006] study of possible sea ice response to ocean heat content anomalies.

---

[1]Woods Hole Oceanographic Institution, Woods Hole, Massachusetts, USA.
[2]Yale University, New Haven, Connecticut, USA.
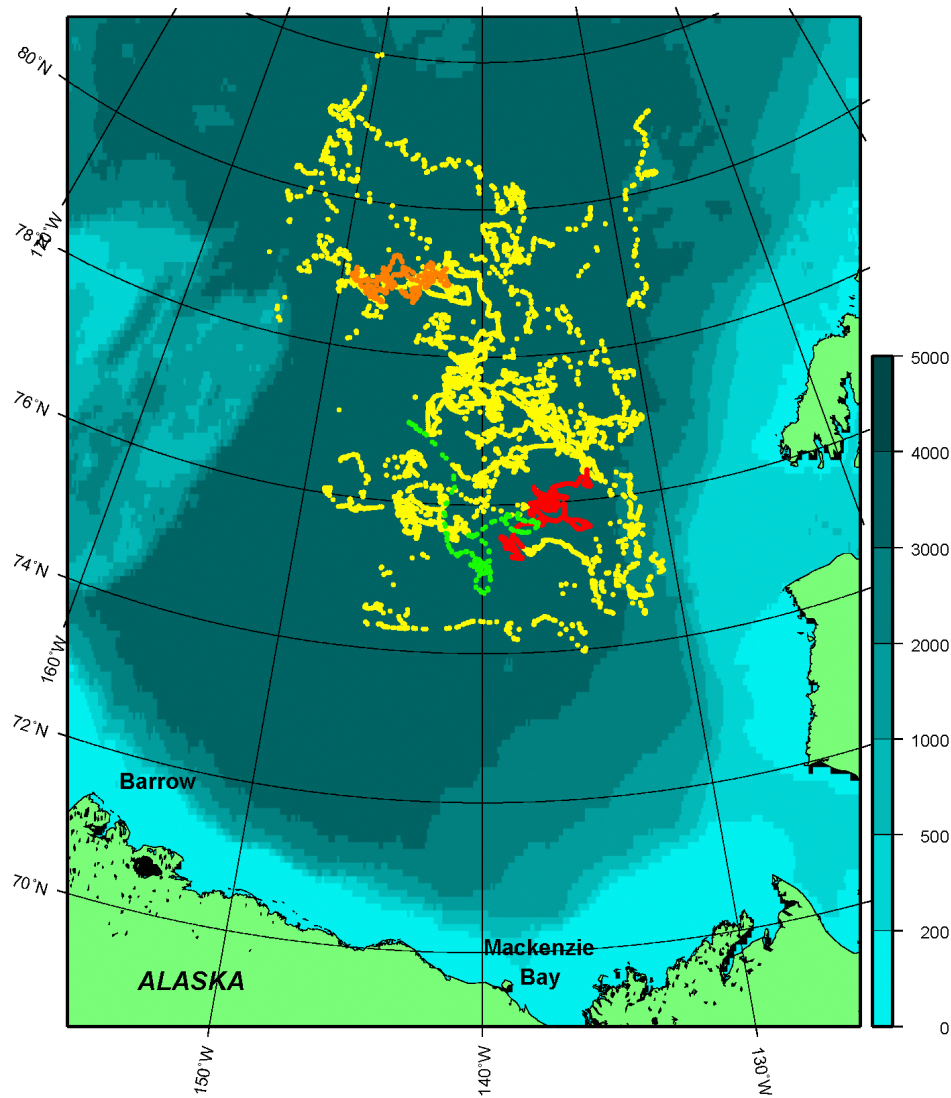[3]Cold Regions Research and Engineering Laboratory, Hanover, New Hampshire, USA.

Figure 1. Distribution of temperature and salinity profiles acquired by ITPs in the central Canada Basin used in the present analysis. Color shading indicates the depth in meters and selected place names are indicated. Special attention is given to profiles from ITP 6 acquired in summer 2007 (green), ITP 3 from winter 2005–2006 (red), and ITP 4 from winter 2006–2007 (orange).

[4] In the following section, the ITP data analyzed here are described and companion IMB data are introduced. Procedures to construct mean seasonal cycles of ML properties are also detailed. To better understand the physical processes causing ML changes, the temporal evolution of select ITP records are examined on seasonal time scale and simulated using an extension to the *Price et al.* [1986] 1-D model. Technical details of the model are given in section 2.3. Results are presented in section 3 and discussed in section 4.

2. Instruments and Methods

2.1. Ice-Tethered Profilers and Ship Observations

[5] High-vertical resolution temperature and salinity profiles were obtained from 10 Ice-Tethered Profilers (ITPs) [*Krishfield et al.*, 2008a] that were deployed and drifted within the Canada Basin between August 2004 and Sep-

tember 2009 (Figure 1 and Table 1). Examination of the data distribution revealed no significant sampling biases in space or time; taken collectively, the data set appears representative of the central Canada Basin in the latter half of the 2000s.

[6] The ITPs were programmed to acquire at least two one-way profiles per day between approximately 7 and 750 m depth initiated at 0000 and 0600 Z. For various reasons, the ITP underwater vehicles do not always reach their programmed top sample depth; treatment of these partial profiles is discussed below.

[7] Nominal ITP profile speed is 0.25 m s^{-1}. Temperature, conductivity, and pressure from the on-board sensors are obtained at 1 Hz during profiling in both directions, though the down-going data are often smeared at the submeter scale due to the sensor sampling in the wake of the vehicle. Corrections for the response characteristics of the sensors were derived as described by *Johnson et al.* [2007] and

Table 1. Deployment Dates and Profile Statistics for the ITPs That Were Deployed in the Canada Basin and Used in the Present Study[a]

ITP	Deployment Date	End Date	No. of Profiles Attempted	No. of Profiles Used Here
1	15 Aug 2005	8 Jan 2007[b]	2043	1344
2	19 Aug 2004	28 Sep 2004	244	168
3	23 Aug 2005	9 Sep 2006[c]	1532	1105
4	3 Sep 2006	17 Aug 2007[b]	698	501
5	7 Sep 2006	7 Sep 2007	1095	651
6	4 Sep 2006	3 Jul 2008	1335	691
8	11 Aug 2007	16 Sep 2009[b]	1570	587
11	9 Sep 2007	8 Jul 2009[d]	1460	1007
13	13 Aug 2007	8 Sep 2008	876	214
18	16 Aug 2007	9 Oct 2008	914	229

[a]Profiles were excluded from the mean seasonal cycle analysis if they failed to resolve the surface mixed layer or lay outside of the study area.
[b]ITP recovered.
[c]ITP destroyed during recovery attempt.
[d]ITP still operational on this date.

Krishfield et al. [2008b]. Predeployment laboratory-derived calibrations were adopted for all temperature and pressure data and the preliminary conductivity estimates. Post-deployment laboratory calibrations of two recovered ITPs documented temperature and pressure offsets after 2–3 years of 1–2 m °C and around 1 db, respectively. We take these as the uncertainties of the final ITP temperature and pressure data. Adjustments to the laboratory conductivity calibrations were derived and applied as detailed by *Krishfield et al.* [2008b] (see also the metadata accompanying the final ITP data products from each instrument accessible from www.whoi.edu/itp and the Cooperative Arctic Data and Information Service archive www.aoncadis.org) to achieve consistency with recently acquired ship-based salinity estimates for the region. The resultant ITP salinity data have an uncertainty (relative to the ship data) of 0.005 or less. The present analysis is based on 1 dbar bin-averaged profile data derived after the above corrections were applied.

[8] The ITP observations from each profile were used to estimate the ML depth, temperature, and salinity. We take the surface mixed layer as that vertical span immediately below the air-sea or ice-sea interface within which fluid parcels experience negligible buoyancy forces while moving vertically. Operationally, the base of the ML was taken as that point in each profile where the potential density relative to 0 dbar first exceeded the shallowest sampled density by 0.01 kg m^{-3}. Considering density noise in the 1 dbar ITP data set as a whole, this was deemed the smallest practical density difference. (A looser density-difference criterion of 0.1 kg m^{-3} applied to the ITP data returned ML depth values that were up to 1–2 m greater than output by our estimator but exhibited similar variability in time.) A profile was discarded if the derived depth of the ML base was within 2 m of the shallowest depth sampled or was less than 10 m. This effectively removed those profiles that did not sample sufficiently shallow to resolve the transition between the homogeneous surface layer and the underlying stratified interior. Approximately 6500 of the available 11,758 profiles from the 10 ITPs satisfied the selection criteria. The majority of discarded profiles were acquired in midsummer when the

Canada Basin ML is frequently thinner than 10 m. The ITP data that passed the selection process consequently yield biased estimates of the mean ML depth in July and August.

[9] The potential temperature (Θ) and salinity of those bins determined to lie within the ML of each profile were averaged, the local freezing temperature was derived using the *Fofonoff and Millard* [1983] algorithm at a pressure of 1 dbar, and the differences with local ML temperature were calculated. In addition, estimates of the stratification at the ML base were derived. To do so, a linear least square fit was made to the potential temperature and potential density relative to 0 dbar from each profile in the 5 m segment immediately below the estimated ML base. All available estimates for each ML parameter were subsequently sorted in time without regard to the year, grouped into month-long periods and the means and standard deviations of the ML properties were estimated.

[10] To assess the magnitude of the summer biases, ship-board CTD data acquired during the annual Beaufort Gyre Observing System (BGOS) cruises [see *Proshutinsky et al.*, 2009] were additionally analyzed. Specifically, using identical methods as detailed above, ML depth and properties were estimated for each station taken in the central Canada Basin on the 2004–2008 cruises, and cruise-averaged values were derived. Several colleagues have cautioned us that the upper-ocean stratification can be disrupted by the icebreaker operations during station work (e.g., L. Rainville, personal communication, 2009). While many of the ship stations, particularly recently, were done in open water, we note the issue. But lacking a systematic way to identify disturbed profiles, we made no attempt to edit or subsample the ship data.

2.2. Ice Mass Balance Buoys

[11] The CRREL (Cold Regions Research and Engineering Laboratory) ice mass balance buoy consists of an assemblage of sensors that measure the thickness of the ice floe (separate sensors sample changes at the top and bottom ice surface) and overlying snow cover where it is deployed as well as the temperature of the air and the temperature profile through the ice. Data from two IMBs that were deployed in the Canada Basin are utilized: IMB 2005B and IMB 2006C. Observations from the latter were previously reported by *Perovich et al.* [2008]. Here only the estimated changes in basal ice floe thickness over time periods of 4–6 months are used. Over a full season, the uncertainty in the estimated amount of basal ice loss/gain is ±1 cm.

2.3. One-Dimensional Model

[12] We conducted specific summer and winter case studies employing a simple ML model to gain insight to the physical processes controlling the central Canada Basin ML properties. The 1-D model applied here (PWP) is a variant of the *Price et al.* [1986] routine (with addition of a linear damping term in velocity, see below) with a simple thermodynamic sea ice layer superimposed. As such, the model is similar to that of *Hyatt* [2006] and can be thought of as a companion to the model of *McPhee* [1999]. Being relatively simple and 1-D, we certainly do not claim that the PWP model accurately captures all the physical processes active in the real ocean-ice system. Rather, we used the model to identify the important factors that might control the evolu-

tion of the Arctic ML and to construct closed ocean-ice heat budgets as a follow-on to *Perovich et al.*'s [2008] analysis of ice thickness changes. The reader is directed to *McPhee*'s [2008] recent monograph for a thorough discussion of ice-ocean boundary layer processes.

[13] Two versions of the model were run. Winter case studies simply involved a single column of ice and ocean. The summer model formulation consisted of two parallel 1-D columns: the first identical to the winter set up and the other, representing the lead subarea of the model, having no ice layer. The lead area fraction for the summer run was specified from observations. After each time step of the two summer submodels, the ocean temperature, salinity, and momentum profiles were mixed horizontally using a weighting given by the lead area fraction. This is an admittedly crude approximation of the complex interaction between the surface waters in leads and those under adjacent ice floes. See, for example, *Skyllingstad et al.* [2005] for a more dynamical study of these processes.

[14] The ocean component of the model had 1 m vertical resolution and extended from the surface to 100 m depth. Model runs were initiated at rest with a specified vertical stratification [$\Theta(z)$, $S(z)$] based on observed ITP profiles as well as specified thickness and (in the summer case) area fraction of the sea ice layer (also based on observations). The model was subsequently integrated forward in time with a 1 h time step to derive the ocean and ice response to specified buoyancy and momentum inputs. The latter were derived from a time series of (observed) sea ice velocity and a quadratic drag law in the (observed) ice-(model) ocean velocity difference. A constant drag coefficient of 5.5×10^{-3} was adopted. Sensitivity runs with a larger drag coefficient were also performed. We note that a uniform drag coefficient is another oversimplification of the real world, and indeed the quadratic form of the drag relationship can be questioned [see, for example, *Shaw et al.*, 2008]. To minimize stress divergence between subdomains of what is effectively a 1-D model, the ice-water stress derived for the ice-covered summer-run column was also applied to the top of the lead submodel column.

[15] Simulations were run with a fixed Coriolis frequency based on the average latitude of the associated ITP observations that each run was based on. Following PWP applications to lower-latitude cases [e.g., *Plueddemann and Farrar*, 2006; *Silverthorne and Toole*, 2009], a linear drag term with a 5 day decay time scale was included in the momentum equation. This term has been included in the PWP framework to crudely account for the radiation of energy (by internal waves) out of the surface layer.

[16] The specified shortwave solar energy flux only entered the ocean in the lead submodel of the summer simulation. The Jerlov Water Type IA double exponential extinction profile (R) taken by PWP was adopted,

$$R(z) = 0.62\,e^{-1.67z} + 0.38\,e^{-0.05z}.$$

The vertical structure of this extinction profile is roughly consistent with the absorption profile reported by *Jackson et al.* [2010]. Following *Perovich et al.* [2008], no other air-sea heat flux terms were considered for the summer simulation. For the winter case studies, a steady ocean heat loss was specified. This heat was removed from the top-most

grid point of the ocean model to mimic ocean heat loss by conduction through the ice and air-sea exchange at leads.

[17] The ice-ocean heat flux (F_{io}) in the model was derived following *Maykut and McPhee* [1995] as

$$F_{io} = \rho c_p c_h u^*(\Theta - \Theta_f),$$

where c_h is a nondimensional heat transfer coefficient (0.006), u^* is the magnitude of the ice-water stress, Θ is the ML potential temperature, and Θ_f is the freezing temperature. Ocean heat fluxed into the ice layer resulted in immediate melting, a flux out of the ice caused freezing. (A uniform heat of fusion of 3.34×10^5 J kg^{-3} and ice density of 900 kg m^{-3} were adopted.) For simplicity, the model ice layer had no salt or sensible heat content. The salinity of the surface ocean layer under the ice varied in response to the basal growth/melting of the ice layer. No other fresh water forcing was applied during these simulations.

[18] The PWP ocean model includes convective adjustment to remove static density inversions and utilizes a Richardson number turbulent mixing closure. At each time step, adjacent ocean layers are mixed vertically until the gradient Richardson number is greater than 1/4. A bulk mixed layer Richardson number criteria is also invoked in PWP to determine the homogeneous (slab) surface layer thickness. This latter step is chiefly one to accelerate the integration time as the gradient Richardson number criteria on its own returns very similar results (J. Tom Farrar, personal communication, 2009). The PWP model code also supports a background vertical diffusivity for temperature, salinity, and momentum. The diffusivity coefficients in these model terms were set negligibly small (10^{-7} m^2 s^{-1}) in order to focus on those mixing processes explicitly resolved by the model.

2.4. Case Studies

[19] Subsections of data from three ITPs were examined in greater detail and simulated with the 1-D model. Specifically, data from ITP 6 during summer 2007 (1 June to 22 September) were examined in a follow-up of *Perovich et al.*'s [2008] analysis of data from the co-located IMB 2006C. As a contrast, winter observations from ITP 3 (1 December 2005 to 1 June 2006) and ITP 4 (1 December 2006 to 1 June 2007) were also studied. ITP 3 was co-located with IMB 2005B; no ice buoy was deployed with ITP 4. Beyond the tie-in with *Perovich et al.* [2008], these three data segments were selected for detailed analysis because the supporting ice floes did not drift very far during these focus periods (Figure 1), reducing but not eliminating signals in the instrument time series due to spatial variability. Time series of ML properties following these drifting ITP instruments were derived as above and depth-time contour plots constructed.

[20] To drive the 1-D model, time series of sea ice drift velocity and the rate of heat exchange with the atmosphere were required. (Fresh water forcing in the model was restricted to that associated with predicted basal ice melt or growth.) Ice velocity time series were derived from the hourly GPS position fixes reported by the ITPs. For the summer simulation, following *Perovich et al.* [2008], we focused on the largest term in the air-sea heat flux budget: the incident shortwave solar energy incident on leads. The
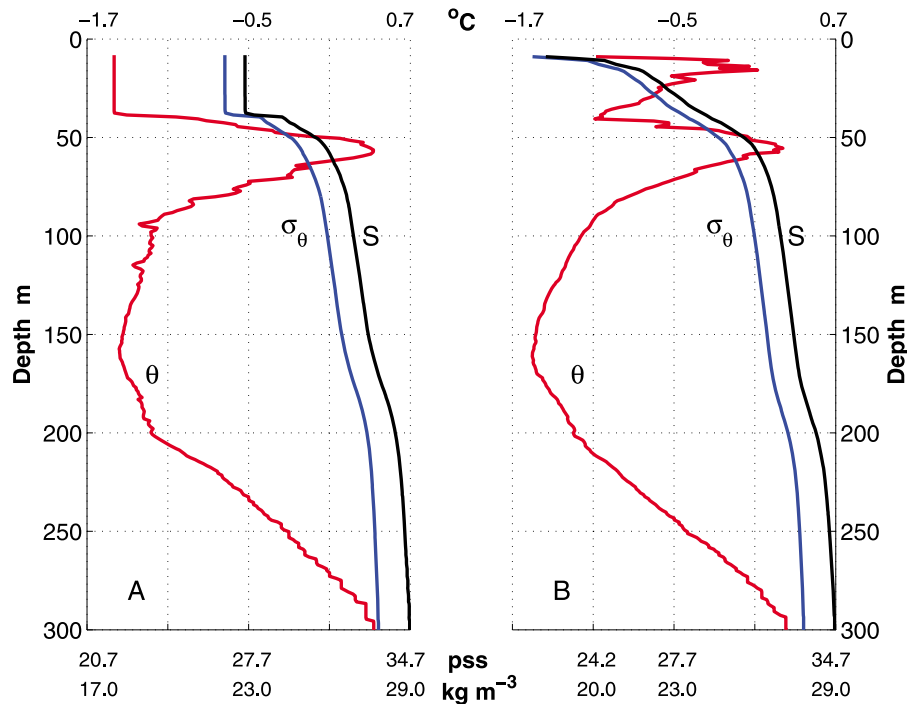
Figure 2. Representative vertical profiles of temperature (red), salinity (black), and potential density anomaly (blue) obtained from ITP 6 on (a) 30 April 2007 and (b) 13 September 2007. These were ITP 6 profiles 475 and 747, respectively; both were taken within 25 km of 76°24′N, 140°45′W.

same incident solar flux and lead-area fraction time series used by *Perovich et al.* [2008] are taken here. The former were extracted from European Center for Medium Range Weather Forecasts operational products, the latter from passive microwave satellite data. The stated uncertainty in the NASA Team 2 algorithm for ice concentration [*Marcus and Cavalieri*, 2000] is about 5%. No uncertainty estimates for the shortwave irradiance were given beyond the statement that the "downwelling shortwave flux data show good agreement with observation and negligible long-term bias."

[21] An average cooling rate for the winter case studies was deduced from the IMB and ITP data. The net cooling experienced by the ice-ocean system can be partitioned into an ice component and an ocean component. IMB 2005B reported approximately 60 and 80 cm of basal ice growth between December and June during the 2005–2006 and 2006–2007 winters, respectively. For the heat of fusion of 3.34×10^5 J kg^{-3} and ice density of 900 kg m^{-3}, these amounts of sea ice growth over 182 days equate with average ocean cooling rates of 11.5 and 15.3 W m^{-2}. Time series of ocean heat content were estimated by integrating ITP profile estimates of $\rho c_p \Theta$ (product of water density, specific heat capacity, and potential temperature) from the surface to the depth of a selected potential isopycnal that lay just below the deepest observed ML in each analysis period. Uniform vertical extrapolation was used to extend profiles from the shallowest sampled level to the surface. Variations in derived ocean heat content due to changes in the depth of the bounding isopycnal were subsequently removed by scaling the original estimates by the ratio of the time-mean depth of the bounding isopycnal to the corresponding local depth value. This treatment is exact for removing variations in derived ocean heat content caused by adiabatic vertical

displacements that increase linearly with depth. Variations in adjusted ocean heat content of less than 5% were observed through the two winter study periods, with neither segment exhibiting a consistent trend in ocean heat content. Thus for simplicity and lacking IMB data from the ITP 4 floe, all winter model runs were driven with a steady cooling rate of 15 W m^{-2} (the cooling rate based on the observed basal growth of sea ice).

[22] Wind stress estimates were used to characterize the mechanical forcing of these case studies. Time series of wind stress on the sea ice following the floes supporting ITPs 3, 4, and 6 were derived from NCAR/NCEP reanalysis sea level pressure data using standard AOMIP (Arctic Ocean Model Intercomparison Project) formulae [see *Proshutinsky and Kowalik*, 2007]. These 6 hourly data were linearly interpolated to the 1 h time step of the 1-D model and ice velocity series.

3. Results

3.1. Representative Vertical Profiles

[23] A quick introduction to the upper ocean stratification in the central Canada Basin is provided by two profiles acquired by ITP 6 on 30 April and 13 September 2007 at nearly the same location (50 km apart). The late winter profile (Figure 2a) shows a well-mixed surface layer extending down to approximately 40 m depth where it is bounded by a very large density gradient (due to salinity). The ML temperature was within a few m°C of the local freezing point, a condition *Shaw et al.* [2009] term an "ice bath." Continuing deeper, the temperature increased to a local maximum centered around 50 m depth. This extremum is an intrusion of Pacific Summer Water (PSW), features
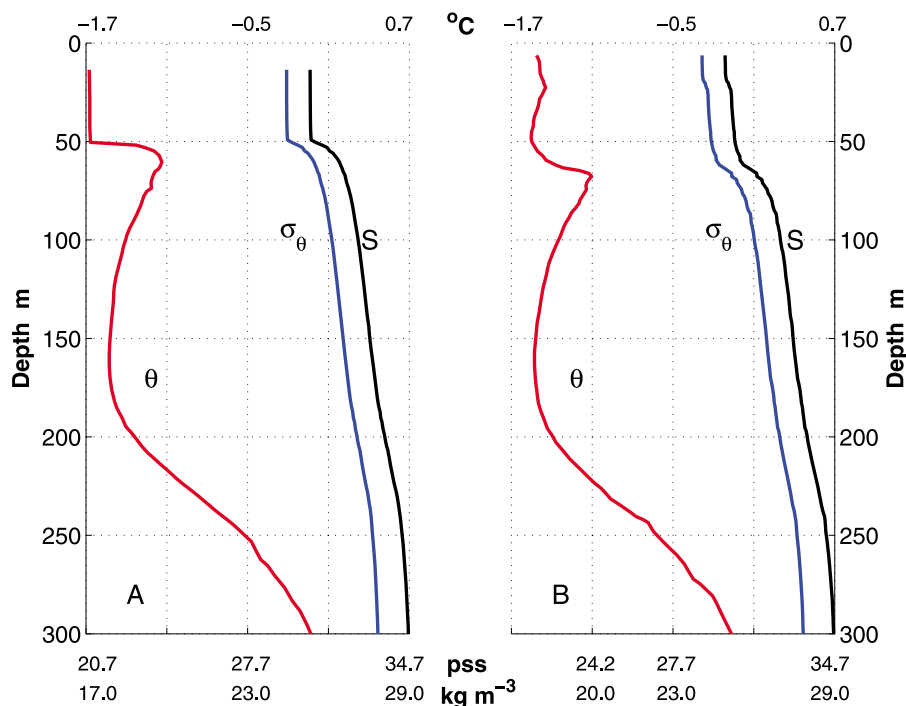
Figure 3. Winter and summer temperature, salinity, and density profile data from the Canada Basin acquired in 1975 during AIDJEX (on the same scales as Figure 2). (a) Station data taken on 28 April at 76°25′N, 144°20′W (94 km from the nominal site of the profiles in Figure 2). (b) Station taken on 23 July at 75°42′N, 145°7′W (141 km from the Figure 2 site).

that are now prominent throughout the central and western Canada Basin [*Shimada et al.*, 2001; *Steele et al.*, 2004]. Below the PSW intrusion, a local temperature minimum was sampled; deeper still, temperature again increased with depth to the core of the Atlantic Water layer that is centered near 400 m depth in this region of the Arctic. Salinity increased with depth through these temperature features providing the stable density stratification.

[24] Greatest differences between the late winter and late summer (Figure 2b) profiles were above ~40 m depth. Curvature in the raw 25 cm resolution temperature and salinity profile data suggest that the base of the well-mixed surface layer was very near the 9 m minimum depth that was sampled on this profile. The salinity at this shallowest sampled level was more than 5 units lower than seen in the winter profile ML. Between the base of the summer ML and the PSW intrusion, a third temperature extrema was seen, a feature *Shimada et al.* [2001] called Summer Mixed Layer Water and *Jackson et al.* [2010] termed the Near-Surface Temperature Maximum (NSTM), which we will use. As will be discussed later, the NSTM is a local, seasonal feature caused by penetrative shortwave solar heating principally through leads [see *Perovich and Maykut*, 1990].

[25] These 2007 upper-ocean conditions were similar to those sampled at the start of the SHEBA ice camp drift 10 years earlier [see *Shaw et al.*, 2009] but strikingly different from the water properties observed in 1975 during the Arctic Ice Dynamics Joint Experiment (AIDJEX). As *McPhee* [2008] has noted (see his Figure 1.3), the central Canada Basin near-surface waters are much warmer and fresher now than 35 years ago. To illustrate this, we display in Figure 3 selected AIDJEX profiles at comparable locations and times

as the ITP 6 profiles. In comparison to 2007, the winter mixed layer in 1975 extended deeper (to ~50 m) with a weaker density jump at its base, the PSW temperature maximum was less pronounced, the contrast with the summer ML salinity was much less (0.4), the summer ML was ~16 m thick, and there was virtually no NSTM. The latter is likely due to the smaller lead area fraction and reduced solar energy reaching the surface in summer 1975 versus 2007.

3.2. Mean ML Seasonal Cycle

[26] Over most of the calendar year, the observed ML in the central Canada Basin is within a few m°C of the local freezing point (Figure 4). However in summer (June-July-August), ML temperatures frequently exceeded the freezing point by 0.1°C–0.2°C. The estimated mean ML depth for the July–August period is just 16 m. Both are biased estimates; recall that the ITPs fail to sample the very shallowest (and warmest) MLs at this time of year. Cruise-mean ML depths estimated from the BGOS data range between 9.5 and 3.2 m with cruise-mean departures of the ML temperatures from the freezing point as high as 0.77 (Table 2). Direct comparison of ship and ITP observations is complicated as the spatial distributions of the two data sets are different. One significant difference is the ship sampled more open water regions than did the ITPs. (The trend of decreasing ice concentration over time is likely responsible for the trend in cruise-mean ML temperatures.) Nevertheless, keeping in mind the possible distortion of the ship CTD data, the overall assessment is that the central Canada Basin in midsummer is characterized by very shallow, warm, and fresh MLs.
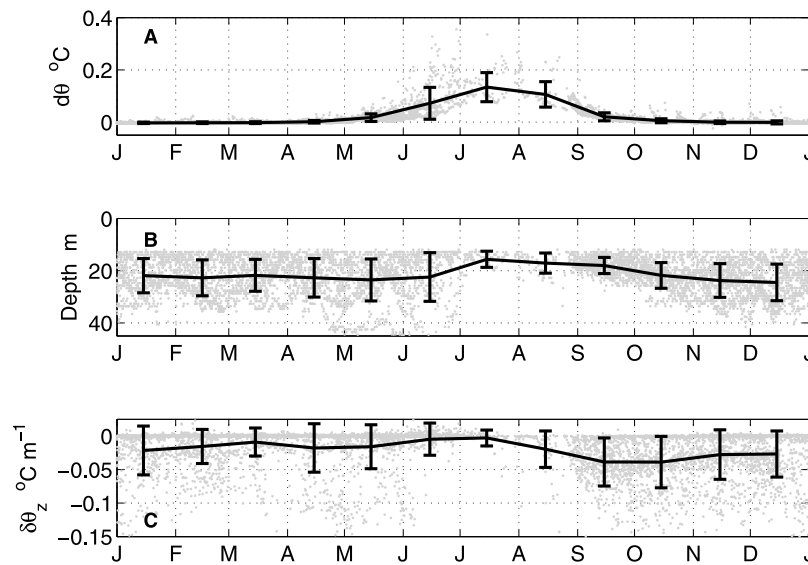
Figure 4. Mean seasonal cycle of central Canada Basin mixed layer temperature departure from the (a) local freezing temperature, (b) mixed layer depth, and (c) vertical potential temperature gradient in the 5 m interval below the mixed layer base based on approximately 5800 ITP profiles. Estimates from individual profiles are marked by gray dots. The black curves connect monthly mean values (reported at the average time of the available estimates); the brackets mark the average plus and minus the estimated standard deviations. Mean estimates for July and August are likely biased estimates as the ITPs often failed to resolve the very shallow and warm mixed layers characteristic of summer.

[27] Notable in the winter observations are the highly variable yet overall relatively shallow ML depths: 60% of the winter samples were shallower than 25 m and averaged just 24 m; ML depth very rarely exceeded 40 m (Figure 5; Figure 2a is an extreme example). These relatively shallow winter MLs are surprising given the strong buoyancy forcing associated with sea ice growth/brine rejection and seasonal Ekman convergence in the Beaufort Gyre [*Proshutinsky et al.*, 2009].

[28] Even before more extensive analysis, Figures 4 and 5 suggest that on seasonal time scales, the heat contained in PSW intrusions centered at and below 50 m depth in the central Canada Basin has little influence on the winter growth of sea ice. The winter ML in this sector of the Arctic seldom, if ever, reaches sufficiently deep to entrain significant PSW heat.

[29] The vertical gradient estimates at the ML base exhibit an interesting bimodal behavior in winter (Figure 4c). Approximately 60% of the vertical density gradient estimates are weaker than 0.05 kg m^{-4} (Figure 5b). Variations in the intensity of the high-gradient samples results in the
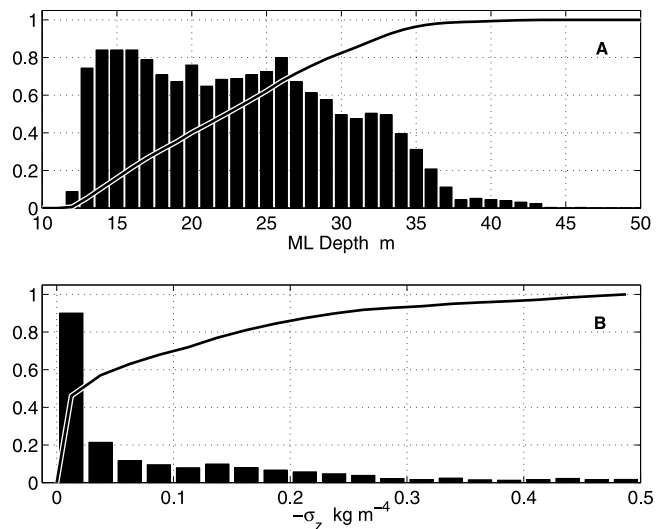

Table 2. Cruise-Mean ML Properties Based on the BGOS Summer Expeditions[a]

Year	No. of stations	H (m)	Θ (°C)	S	$\Theta - \Theta_f$ (°C)
2004	21	7.0	−1.40	28.3	0.14
2005	27	5.2	−1.31	27.7	0.20
2006	30	9.5	−1.27	26.5	0.17
2007	50	3.2	−0.80	24.5	0.53
2008	44	6.9	−0.64	26.0	0.77

[a]For each ship station in the study region, the ML properties were estimated. Reported are the cruise-mean ML depth (H), ML potential temperature (Θ), salinity (S), and departure from the local freezing point ($\Theta - \Theta_f$).

Figure 5. (a) Scaled histograms and cumulative probability distributions of wintertime observations (November–April) of mixed layer depth and (b) the vertical density gradient in the 5 m below the mixed layer base in the central Canada Basin. The base of the ML was taken as that point in a given profile where the potential density relative to 0 db first exceeded the shallowest sampled density by 0.01 kg m^{-3}. The small number of ML depth estimates shallower than 12 m is an artifact of the profile editing procedure (see text).
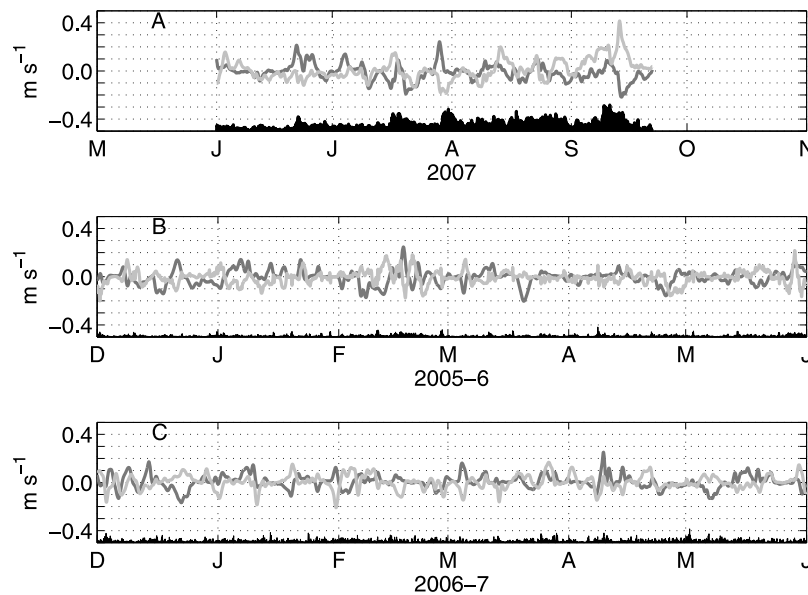
Figure 6. Time series of ice-floe velocities for the three case studies. The two components of low-pass-filtered velocity (filter cutoff period of 24 h) and amplitude of the high-pass-filtered oscillations are presented, based on hourly position fixes by the ITPs. The black curves are the low-passed zonal velocity component while the gray curves are the low-passed meridional component. The black shaded curves at the bottom of each panel indicate the amplitude of the high-passed oscillations (offset by −0.5 m s^{-1}): (a) summer 2007, ITP 6; (b) winter 2005–2006, ITP 3; (c) winter 2006–2007, ITP 4.

broad probability distribution at greater stratifications. (That bimodal behavior is also seen in the base potential temperature gradients, see Figure 4c, which rules out salinity noise as causing spurious density signals and erroneous ML depth values. Rather, these base potential temperature and potential density gradient estimates have a 0.89 correlation based on 3900 independent samples.) The winter ML depth and base gradient samples are significantly correlated (correlation coefficient of 0.50, with deeper MLs corresponding to stronger stratification). This behavior is not an artifact of grouping profiles from different areas and years. As will be shown later, individual ITP time series show profiles with relatively deep MLs interspersed with profiles exhibiting thinner MLs.

3.3. Case Study: Summer

[30] As *Perovich et al.* [2008] described, the ice floe that supported the ITP 6/IMB 2006C instrument cluster lost 2.1 m of thickness by bottom melting and approximately 60 cm by surface melting during the summer of 2007. The upper ocean salinity change sampled by ITP 6 is quite consistent with this; based on the profiles of Figure 2, a dilution of 2.3 m of fresh water is required to account for the observed 1.48 salinity change averaged over the upper 40 m of the ocean. Perovich and colleagues demonstrated that there was more than enough solar energy incident on leads surrounding this ice floe to account for the bottom melt. Here we use the 1-D PWP model with reference to the ocean and ice observations to derive a closed ice and ocean heat budget.

[31] Inputs to the model for the study time period of 1 June to 22 September 2007 consisted of an initial temperature and salinity profile acquired on June 1 (very similar to that in Figure 2a except that the winter ML was capped by a very weak seasonal pycnocline at 10 m), and time series

of ice floe velocity (Figure 6a), incident shortwave solar flux and ice/lead area fraction for the region surrounding the floe (Figure 7), all interpolated linearly to the 1 h model time step. The ice floe velocity data from this period exhibit pronounced inertial ringing with amplitude approaching 20 cm s^{-1} several times during the summer. Total ice floe speed peaked at 50 cm s^{-1} during a storm late in the focus period (Figure 6a). The extended inertial ringing suggests that internal ice stresses were weak during the summer, as one might expect with so much open water in the region (Figure 7b).

[32] The 1-D model simulation results are in reasonably good agreement with the observations (Figure 8) though much more variability was observed by the drifting ITP than simulated by the model. Over the study period, the specified ocean heating rate (shortwave radiation crossing the air-sea interface) averaged 65 W m^{-2}. (This and subsequent flux estimates are area-weighted by the ice/lead area fraction.) Of this, 50 W m^{-2} went to bottom melt with the remaining 15 W m^{-2} causing an increase in ocean heat content. This means ice-ocean heat flux is a factor of three greater than what *Shaw et al.* [2009] estimated during the summer segment of the SHEBA drift. The 1-D model predicts an area-weighted bottom melt of 2.1 m over the simulation period. Note that the ice column of the 1-D model experienced nearly 3 m of melt; the 2.1 m figure derives from the ice area fraction weighting. This discrepancy with what IMB 2006C observed, which is arguably representative of the ice-covered column of the 1-D model, can perhaps be rationalized by attributing some of the ocean heat flux to lateral melting [e.g., *Skyllingstad et al.*, 2005].

[33] Most of the 15 W m^{-2} of ocean warming in the simulation manifested as a NSTM just below the ML, similar to what was observed by ITP 6 (Figure 8c). (The model
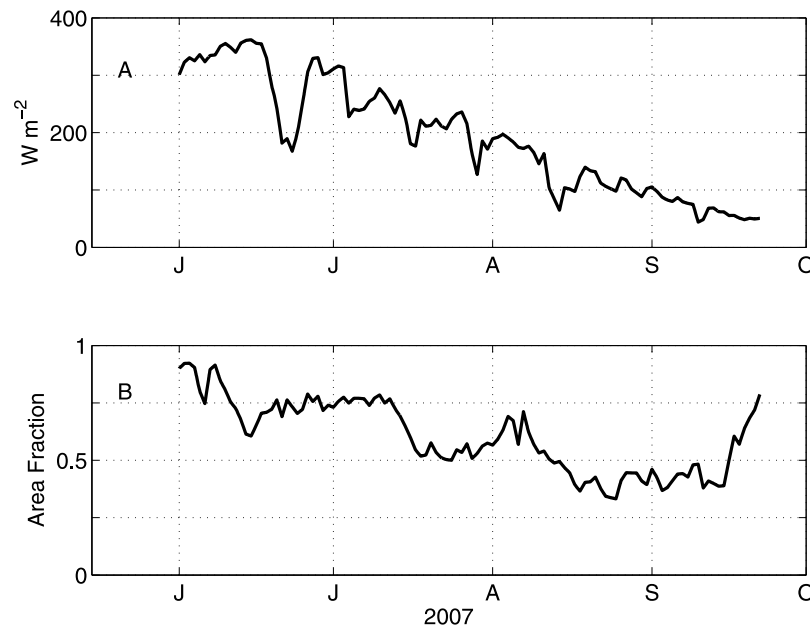
Figure 7. Time series of (a) incident shortwave solar heat flux and (b) lead area fraction for the summer 2007 case study. These same time series were used by *Perovich et al.* [2008].
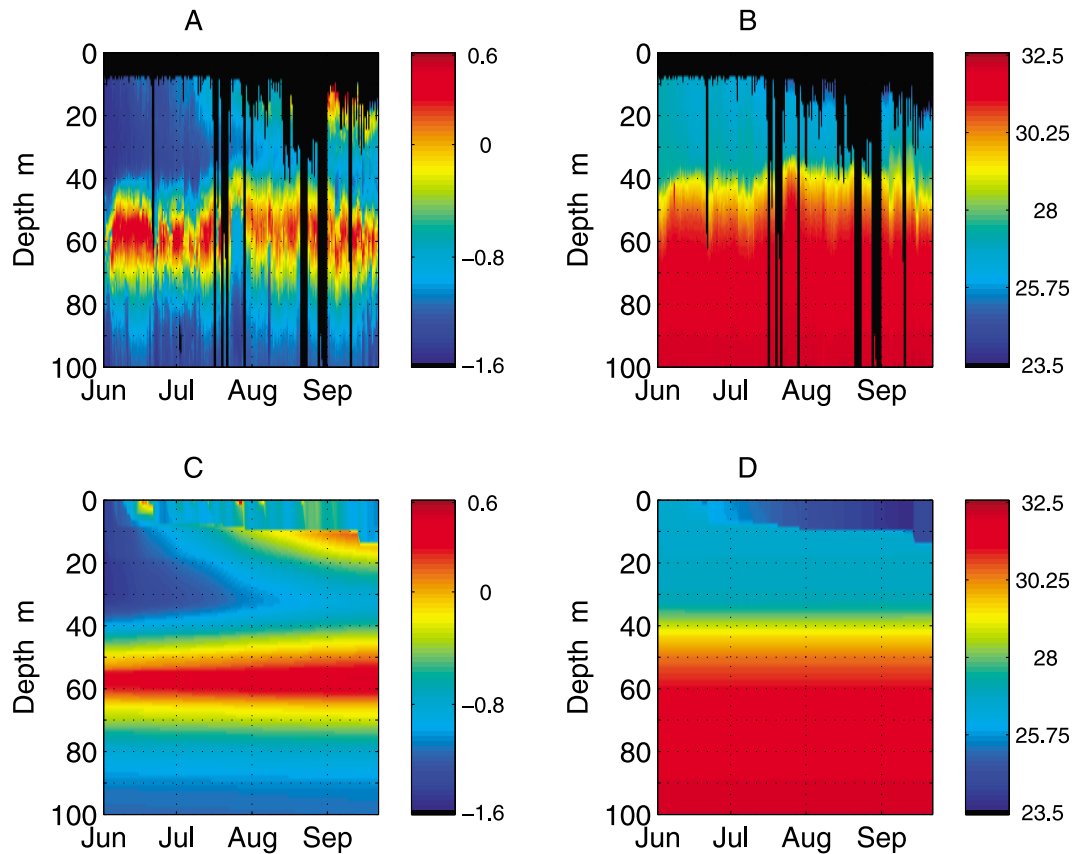

Figure 8. Depth-time contour plots of the observed and modeled upper ocean temperature and salinity for the summer 2007 case study: (a, b) observations from ITP 6; (c, d) PWP model output. The base temporal resolution of the ITP data was two profiles per day; the model output has 1 h resolution. A black mask is used in Figures 8a and 8b to indicate depths/times that the ITP failed to sample.
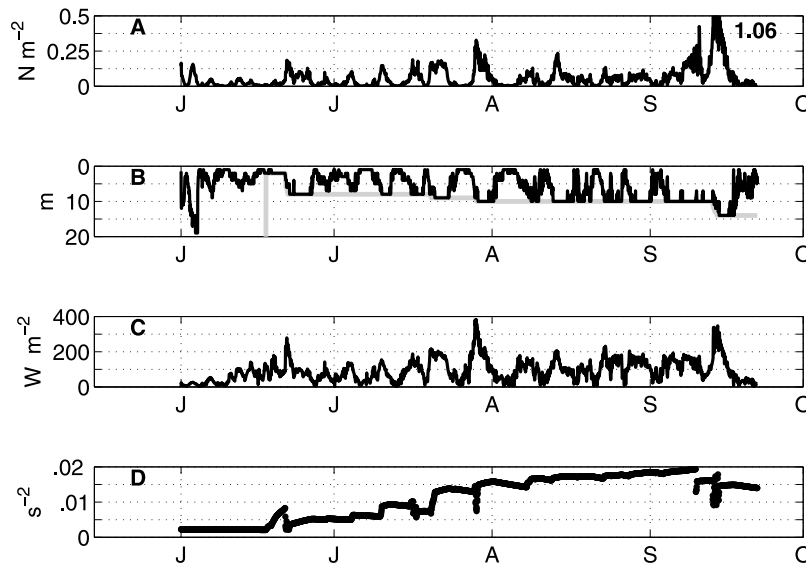
Figure 9. Time series of 1-D model parameters for the summer 2007 case study. (a) Derived ice-water stress. Note the peak value during the mid-September event (1.06 N m^{-2}) is off the scale of the figure. (b) Depth of the ML base. The gray curve marks the depth of the maximum density stratification in the model water column. For the first 2 weeks of the simulation, the strongest vertical stratification was at 40 m depth, remnant in the initial condition profile of the previous winter ML base. (c) Derived heat flux from the ocean to the sea ice layer. (d) Squared buoyancy frequency at the depth of maximum stratification.

warming of the PSW layer seen in Figure 8c is also due to penetrative shortwave radiation.) The buoyancy source provided by the melting ice was a significant impediment to ML deepening throughout the simulation. After an initial stress-driven deepening episode in the first 2 days of the run that saw the ML extend to 19 m (Figure 9), for most of the following study period the model ML varied between 1 and 10 m despite stress events of comparable or greater magnitude. Each stress event was accompanied by a pulse of heat flux to the ice layer that caused melting. The surface stress was usually large enough to mix that buoyancy down to around 10 m, but no deeper. Consequently, the stratification around 10 m depth increased with time such that the major stress event at the end of the run could drive only 4 m of additional deepening and leave a ML just 14 m thick.

[34] In the model, the ocean-ice heat flux is proportional to the ice-water stress and departure of the surface temperature from the freezing point. Not surprisingly therefore, the time series of ice-ocean stress and heat flux are highly correlated, with the latter exhibiting peak events reaching 100–200 W m^{-2} coinciding with wind-driven surges in ice velocity when the magnitude of the ice-water stress reached 0.1–0.2 N m^{-2} (Figure 9). Shortly after each of these events, inertial oscillations in the ML phase lock with the inertial ice motions and the ice-water stress and heat flux fall towards zero. This phase-locking behavior explains the relative insensitivity of the model results to the adopted drag coefficient between the ice and water. Doubling the drag coefficient while keeping all other model parameters, the same resulted in a near doubling of the work done by ice drag on ML currents but just a 10% increase in area-averaged ice melt over the simulation period. The heat to support this added melt came from the NSTM layer, which was unrealistically fully entrained into the ML by enhanced shear

mixing. The ML thickness in this double-drag run was about twice the standard run, but never deeper than 30 m. The thicker ML compensated for the greater ice drag work, yielding ML currents that were very comparable to the standard run.

3.4. Case Study: Winter

[35] To better understand what limits Canada Basin ML depths to less than 40 m, winter 1-D simulations were performed as described in section 2.3. For each year case, model runs were initiated with two different observed temperature and salinity profiles to explore sensitivity to the initial stratification (particularly ML depth). For the winter 2005–2006 runs, ITP 3 profiles 395 (ML depth 39 m) and 501 (18 m) were taken, and for winter 2006–2007, ITP 4 profiles 179 (41 m) and 211 (13 m) were used. In all cases, the simulations were begun on 1 December of the respective year and run for 6 months. In contrast to the summer case, the ice floe speeds for these winter cases were about factor of two smaller and exhibited much less inertial behavior (Figure 6) [see also *McPhee*, 1978]. Both are probably the result of significant internal ice stresses as the wind stress on the ice for these winter periods was about twice that of the summer case. (Simulation period averages of the wind stress magnitudes were 1.14 and 1.03 N m^{-2} for the ITP 3 and 4 winter case studies, respectively, as compared to 0.54 N m^{-2} for the ITP 4 summer period.) In all cases, a uniform ocean cooling of 15 W m^{-2} was applied, as described in section 2.4.

[36] The bulk of the imposed cooling in these winter simulations went into basal ice growth: ~70 cm over the study periods. Ocean heat content decrease accounted for no more than 10% of the applied cooling, reflecting the facts that initial condition ML temperatures were at the freezing
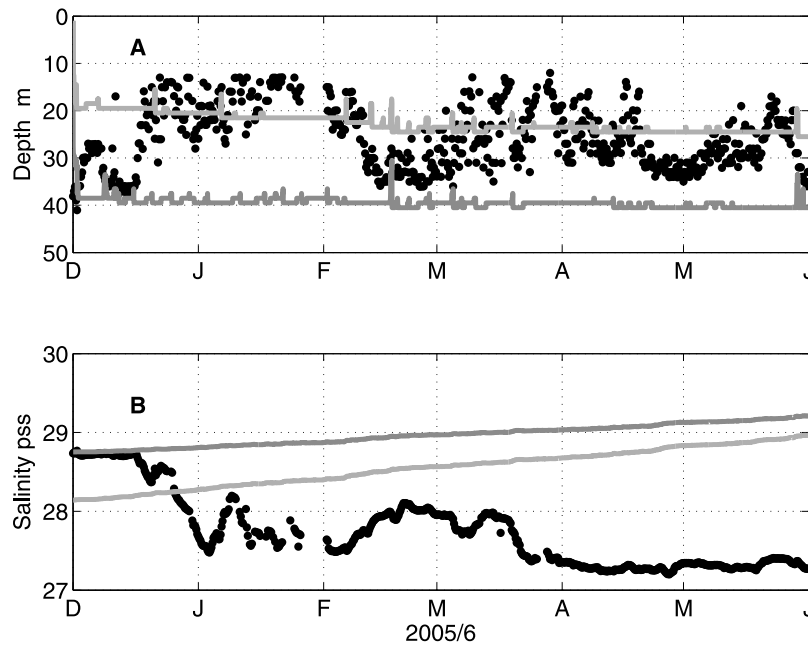
Figure 10. Time series of observed and modeled (a) mixed layer depth and (b) mixed layer salinity for the winter 2005–2006/ITP 3 case study. Individual ITP profile results are indicated by dots; model output for two runs initialized with different temperature and salinity profiles are indicated with the gray lines.

point and only a small amount of shear mixing and ML deepening occurred in these runs. Virtually no ML deepening was simulated for the runs where the initial ML depth was around 40 m (Figures 10 and 11). Shear mixing about the ML base in these cases only extended down another 5–45 m depth, similar to what *Shaw et al.* [2009] observed. The predicted simulated ML deepening in the model runs initiated with relatively thin ML depths was at most 10 m,

with mixing influences again extending down no more than 5 additional meters.

[37] Notably, the observed ML properties show much more variability than was simulated in the winter model runs (Figures 10 and 11). Observed ML depths were at times comparable to those in the simulations but often shallower by ~10 m. Model ML salinities increased with time in all four simulations, reflecting the growth of sea ice and entrainment at the ML base. Observed ML salinities were
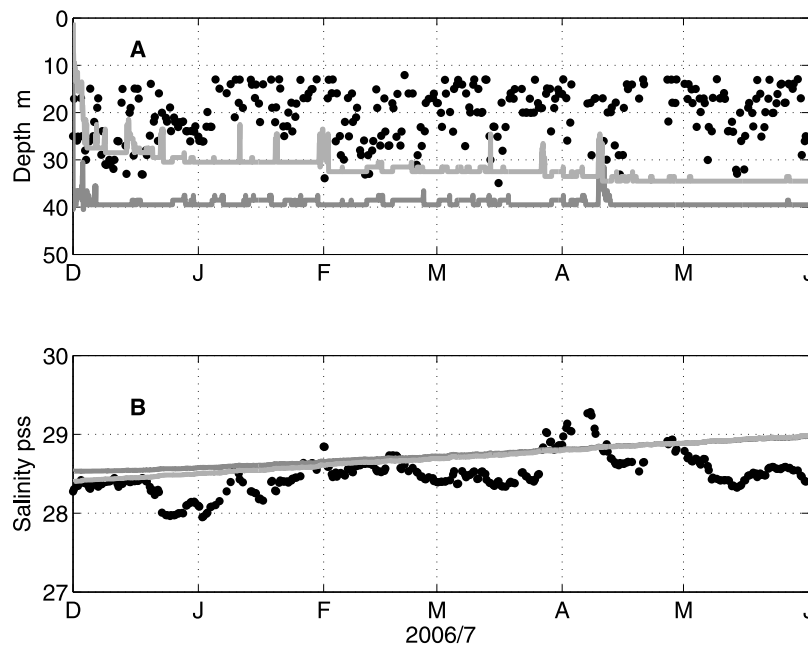

Figure 11. As in Figure 8, but for the winter 2006–2007/ITP 4 case study.

more variable and in the ITP 3 case, actually decreased over the 6 month study period (Figure 10b). Given that IMB 2005B showed sea ice growth over this time, the observed decrease in ML salinity must have been the result of spatial variability in ML salinity that was sampled when the ice floe supporting ITP 3/IMB 2005B moved relative to the water. These observations demonstrate a limitation when combining IMB data from a given ice floe with observations of the underlying ML that is free to move relative to the ice. Interestingly, ITP 4 drifted comparable distances the following winter (Figure 1) but saw smaller variations in ML salinity and no consistent trend. Evidently the fresh water content anomalies of the central Beaufort Gyre [*Proshutinsky et al.*, 2009] where ITP3 drifted during the winter 2005–2006 are characterized by large horizontal gradients.

4. Discussion

[38] Echoing the findings of *Shaw et al.* [2009], one interesting prediction of the 1-D model was the limited thickness of the mixing zone at the ML base; it extended below the ML base no more than 5 m. This zone in the PWP model is dictated by the gradient Richardson number: the squared ratio of the buoyancy frequency to the shear magnitude. The latter depends on the intensity of the ML currents, which in turn is a function of the work done on ML currents by the surface stress (wind and/or ice drag). The 1-D model output may be used to estimate one element of that work, specifically that done by the surface stress acting on the vertically averaged, ageostrophic ML flow. Sidestepping the complexities of vertical structure in the turbulent boundary layer (as is appropriate when considering the PWP slab-type ML), it can be shown (by constructing an equation for the time rate of change of the depth-averaged kinetic energy by vertically integrating the linear horizontal momentum equations from the surface to the ML base and then taking the dot product with the vertically averaged horizontal velocity) that this work contribution is given by the dot product of the surface stress and the depth-averaged ML velocity. Summer and winter case 1-D model estimates of the ice-water stress and depth-averaged ML velocity were extracted to make these calculations, yielding average work estimates for the respective analysis periods of 0.46 mW m^{-2} (summer case) and 0.02–0.03 mW m^{-2} (winter cases). The model estimates for the work done on the depth-averaged near-inertial ML currents ranged from 0.01 to 0.02 mW m^{-2}.

[39] Apart from times when the ML was deepening, most of the energy put into the depth-averaged ML currents was dissipated in the model by the linear decay term, included in the PWP model to crudely account for ML energy loss by internal wave radiation. For reference, *Halle and Pinkel* [2003] estimated downward near-inertial internal wave energy fluxes in the western Canada Basin during winter 1993–1994 that were typically around 0.02 mW m^{-2} with a peak value during one wave event of 0.15 mW m^{-2}. In contrast, typical values estimated for the work done by the wind on near-inertial ML motions at mid-latitudes and in the Southern Ocean are on the order 1 mW m^{-2} [e.g., *D'Asaro*, 1985; *Alford*, 2001, 2003; *Plueddemann and Farrar*, 2006; *Silverthorne and Toole*, 2009; *Elipot and Gille*, 2009] with estimates for the wind work on the full ageostrophic ML

currents in Southern Ocean suggested to be an order of magnitude greater [*Elipot and Gille*, 2009]. While a full analysis of the ML energy budget is beyond the scope of the present study, these results may help explain why the Arctic internal wave field is so much weaker than that at more southerly latitudes [e.g., *Levine et al.*, 1985; *Morison*, 1986; *D'Asaro and Morehead*, 1991; *Pinkel*, 2008]: it simply is not forced very strongly.

[40] Based on the ITP observations of ML base gradients, we can estimate the magnitude of turbulent diapycnal diffusivity that would be required in order for sub-ML ocean heat to contribute substantively to the seasonal ML heat budgets of our case studies. To achieve a turbulent ocean flux into the ML of comparable magnitude to the summer case shortwave heat flux that averaged 65 W m^{-2}, a vertical diffusivity of 13×10^{-4} m^2 s^{-1} acting on the observed summer-mean vertical temperature gradient at the ML base of -1.2×10^{-2}°C m^{-1} would be required. Similarly, to achieve a diffusive flux at the ML base with amplitude comparable to the 15 W m^{-2} of cooling adopted in the winter model runs given the observed winter-average ML base temperature gradient of -2.0×10^{-2}°C m^{-1}, a diffusivity of 2×10^{-4} m^2 s^{-1} is needed. These diffusivity values are several orders of magnitude greater than what has been reported for the stratified upper Arctic Ocean away from bathymetric features and eddies [e.g., *Padman and Dillon*, 1987; *Padman et al.*, 1990; *Zhang and Steele*, 2007; *Shaw et al.*, 2009; P. Winsor and L. Rainville, personal communication, 2009]. Thus, consistent with the analyses of *Maykut and McPhee* [1995] and *Shaw et al.* [2009], we conclude that on seasonal time scales, stratification barriers at 30–40 m depth are presently isolating the surface waters and sea ice in the central Canada Basin from the influences of deeper heat anomalies. Internal wave breaking is often invoked to support background levels of turbulent mixing. The observed low levels of turbulent dissipation in the Arctic imply that whatever internal wave energy is able to radiate out of the Canada Basin ML must propagate down through the shallow pycnocline with little loss to turbulent mixing.

[41] The above conclusions appear at first to be at odds with *Shimada et al.* [2006], who reported a correlation between the spatial distribution of shallow PSW heat anomalies and changes in the sea ice distribution in the far western Canada Basin and Chukchi Cap region. The disagreement seems in part one of terminology. *Shimada et al.* [2006] focus on the heat contained in waters with salinity between 31 and 32, the subcomponent of PSW *Shimada et al.* [2001] termed Eastern Chukchi Summer Water (ECSW). Those regions where, after 1997, anomalously warm ECSW appeared at 20–60 m depth (immediately below the ML), were subsequently seen to experience reduced sea ice cover. However, in the central Canada Basin this PSW component sits below 50 m depth (having been subducted below the very fresh surface layers) and, based on the present results, appears largely insulated from the upper ocean at present. Perhaps weaker density stratification in the west, as was reported by *Shaw et al.* [2009], allows the ML in *Shimada et al.*'s [2006] response region to entrain significant ECSW heat. Yet, *Shaw et al.* [2009] estimated heat fluxes at the ML base only on the order 1 W m^{-2} for the SHEBA drift segments over the Northwind Ridge and Chukchi Cap, com-

parable to what they observed in the central Canada Basin. Thus, it remains unclear to us what physical processes caused the correlated PSW-sea ice changes reported by *Shimada et al.* [2006].

[42] In contrast, heat in the NSTM layer of the central Canada Basin (the warm layer immediately below the ML, perhaps analogous to *Shimada et al.*'s [2006] situation) can be entrained into the ML in fall (September–November) and can act to significantly delay the onset of seasonal sea ice growth. Indeed, our summer case study average rate of ocean heat content change of 15 W m^{-2} that manifested as a NSTM is comparable to our inferred winter case average cooling rate based on the observed 60–80 cm of winter ice growth. While our summer 2007 case was an extreme example, it does highlight the effectiveness of the ice-albedo feedback that can result in ice thinning on an annual basis. Large lead area fractions contributed greatly to the summer 2007 case ocean heat gain and related ice melt. The present modeling approach that specified lead area obviously cannot address the root cause of the dramatic sea ice melt reported by *Perovich et al.* [2008] and examined in our summer 2007 case study.

[43] One of the major discrepancies between the winter observations and our companion model runs was variability in ML depth. The observations from the two winter case study periods show MLs varying from ∼10 m to 30–40 m depth, often on time scales of a few days (Figure 10). Moreover, there was a tendency for the simulations to unrealistically sustain initialized deep MLs. The real ocean ML is driven by highly variable buoyancy forces in both time and space (the latter dominated by lead processes). ITPs that drift relative to the ML would sample the resulting ML variability. Adoption of a steady ocean cooling rate in the 1-D simulations and absence of lateral advection effects most certainly minimized temporal variability in the model output. Another possible explanation for the observed variability is baroclinic instability of adjacent ML columns with slightly different densities and/or ML depths (another process not represented in the 1-D model). As *Boccaletti et al.* [2007] discuss in their review paper, this ML restratification process is believed to be very efficient at mid-latitudes and acts to limit localized deep convection. It would be interesting to explore these ML processes in an Arctic setting with its added complication of a sea ice cover.

[44] The anecdotal finding here that Canada Basin MLs have warmed and freshened in recent years, resulting in enhanced stratification at the ML base, raises questions about the future. One of our reviewers offered us a thought-provoking interpretation of these ML changes in terms of the ML turbulent kinetic energy (TKE) budget. Paraphrasing the reviewer comments: changes in the vertical temperature and salinity stratification since 1975 has resulted in an approximate doubling in "cost" to the ML TKE budget of turbulent heat entrainment at the ML base. Assuming all other dimensional forcing scales of the TKE budget are the same, this stratification increase implies only about half as much sub-ML heat is currently being entrained into the ML. On the other hand, the Canada Basin ML appears to be thinning over time. Concentration of ML turbulence due to layer thinning may eventually compensate for the stratification increase, resulting in greater turbulent heat entrainment.

[45] While PSW heat appears not to be presently influencing the central Canada Basin ML and sea ice on seasonal timescales, it is conceivable that over longer periods that heat could become significant. After all, the PSW heat now entering the central Canada Basin cannot simply disappear. Rather it is presently being stored in the ocean as intrusions in the 40–100 m depth range at sufficient magnitude that if this heat were to somehow be introduced into the ML, it could melt about 1 m of ice. However, it is not obvious what physical mechanisms might allow the ML to rapidly tap that heat. Additional winter 1-D model runs initialized with profiles in which the low-salinity cap in the upper 50 m was artificially removed failed to entrain significant PSW heat, even when more than 3 times the ocean cooling rate and 10 times the mechanical work of the standard winter model runs were applied to the ML. It thus seems for the near future, the impact to sea ice of PSW heat in the central Canada Basin will be limited.

References

Alford, M. H. (2001), Internal swell generation: The spatial distribution of energy flux from the wind to mixed layer near-inertial motions, *J. Phys. Oceanogr.*, *31*, 2359–2368.

Alford, M. H. (2003), Improved global maps and 54-year history of wind-work on ocean inertial motions, *Geophys. Res. Lett.*, *30*(8), 1424, doi:10.1029/2002GL016614.

Boccaletti, G., R. Ferrari, and B. Fox-Kemper (2007), Mixed layer instabilities and restratification, *J. Phys. Oceanogr.*, *37*, 2228–2250.

D'Asaro, E. A. (1985), The energy flux from the wind to near-inertial motions in the surface mixed layer, *J. Phys. Oceanogr.*, *15*, 1043–1059.

D'Asaro, E. A., and M. Morehead (1991), Internal waves and velocity fine structure in the Arctic Ocean, *J. Geophys. Res.*, *96*(C7), 12,725–12,738, doi:10.1029/91JC01071.

Elipot, S., and S. T. Gille (2009), Estimates of wind energy input to the Ekman layer in the Southern Ocean from surface drifter data, *J. Geophys. Res.*, *114*, C06003, doi:10.1029/2008JC005170.

Fofonoff, N. P., and R. C. Millard Jr. (1983), Algorithms for computation of fundamental properties of seawater, *Unesco Tech. Pap., Mar. Sci.*, *44*, 53 pp.

Halle, C., and R. Pinkel (2003), Internal wave variability in the Beaufort Sea during the winter of 1993/1994, *J. Geophys. Res.*, *108*(C7), 3210, doi:10.1029/2000JC000703.

Hyatt, J. (2006), *Wind, Sea Ice, Inertial Oscillations and Upper Ocean Mixing in Marguerite Bay, Western Antarctic Peninsula: Observations and Modeling*, Ph.D. dissertation, MIT/WHOI Joint Program, 171 pp.

Jackson, J. M., E. C. Carmack, F. A. McLaughlin, S. E. Allen, and R. G. Ingram (2010), Identification, characterization and change of the near-surface temperature maximum in the Canada Basin, 1993–2008, *J. Geophys. Res.*, *115*, C05021, doi:10.1029/2009JC005265.

Johnson, G. C., J. M. Toole, and N. G. Larson (2007), Sensor corrections for Sea-Bird SBE-41CP and SBE-41 CTDs, *J. Atmos. Ocean. Technol.*, *24*, 1117–1130.

Krishfield, R., J. Toole, A. Proshutinsky, and M.-L. Timmermans (2008a), Automated Ice-Tethered Profilers for seawater observations under pack ice in all seasons, *J. Atmos. Ocean. Technol.*, *25*, 2091–2095.

Krishfield, R., J. Toole, and M.-L. Timmermans (2008b), ITP Data Processing Procedures, unpublished manuscript (Available from http://www.whoi.edu/page.do?pid=23096).

Levine, M. D., C. A. Paulson, and J. H. Morison (1985), Internal waves in the Arctic Ocean: Observations and comparison with lower latitude climatology, *J. Phys. Oceanogr.*, *15*, 800–809.

Marcus, T., and D. J. Cavalieri (2000), An enhancement of the NASA Team sea ice algorithm, *IEEE Trans. Geosci. Remote Sens.*, *38*, 1387–1398.

Maykut, G. A., and M. G. McPhee (1995), Solar heating of the Arctic mixed layer, *J. Geophys. Res.*, *100*(C12), 24,691–24,703, doi:10.1029/95JC02554.

McPhee, M. G. (1978), Simulation of inertial oscillations in drifting pack ice, *Dyn. Atmos. Oceans*, *2*, 107–122.

McPhee, M. G. (1999), Parameterization of mixing in the ocean boundary layer, *J. Mar. Syst.*, *21*, 55–65.

McPhee, M. (2008), *Air-Ice-Ocean Interaction: Turbulent Ocean Boundary Layer Exchange Processes*, ISBN 978-0-387-78334-5, 215 pp., Springer.

Morison, J. H. (1986), Internal waves in the Arctic Ocean: A review, in *Geophysics of Sea Ice*, edited by N. Untersteiner, 1163–1183, Plenum, New York, NY.

Padman, L., and T. M. Dillon (1987), Vertical heat fluxes through the Beaufort Sea thermohaline staircase, *J. Geophys. Res.*, *92*(C10), 10,799–10,806, doi:10.1029/JC092iC10p10799.

Padman, L., M. Levine, T. Dillon, J. Morison, and R. Pinkel (1990), Hydrography and microstructure of an Arctic cyclonic eddy, *J. Geophys. Res.*, *95*(C6), 9411–9420.

Perovich, D. K., and G. A. Maykut (1990), Solar heating of a stratified ocean in the presence of a static ice cover, *J. Geophys. Res.*, *95*(C10), 18,233–18,245, doi:10.1029/JC095iC10p18233.

Perovich, D. K., J. A. Richter-Menge, K. F. Jones, and B. Light (2008), Sunlight, water, and ice: Extreme Arctic sea ice melt during the summer of 2007, *Geophys. Res. Lett.*, *35*, L11501, doi:10.1029/2008GL034007.

Pinkel, R. (2008), The wavenumber-frequency spectrum of vortical and internal wave shear in the Western Arctic, *J. Phys. Oceanogr.*, *38*, 277–290.

Plueddemann, A. J., and J. T. Farrar (2006), Observations and models of the energy flux from the wind to mixed-layer inertial currents, *Deep Sea Res., Part II*, *53*, 5–30.

Price, J., R. Weller, and R. Pinkel (1986), Diurnal cycling: Observations and models of the upper ocean response to diurnal heating, cooling and wind mixing, *J. Geophys. Res.*, *91*(C7), 8411–8427, doi:10.1029/JC091iC07p08411.

Proshutinsky, A. Y., and Z. Kowalik (2007), Preface to special section: Arctic Ocean Model Intercomparison Project (AOMIP) studies and results, *J. Geophys. Res.*, *112*, C04S01, doi:10.1029/2006JC004017.

Proshutinsky, A., R. Krishfield, M. Timmermans, J. Toole, E. Carmack, F. McLaughlin, W. J. Williams, S. Zimmermann, M. Itoh, and K. Shimada (2009), Beaufort Gyre freshwater reservoir: State and variability from observations, *J. Geophys. Res.*, *114*, C00A10, doi:10.1029/2008JC005104.

Richter-Menge, J. A., D. K. Perovich, B. C. Elder, K. Claffey, I. Rigor, and M. Ortmeyer (2006), Ice mass balance buoys: A tool for measuring and attributing changes in the thickness of the Arctic sea ice cover, *Ann. Glaciol.*, *44*, 205–210.

Shaw, W. J., T. P. Stanton, M. G. McPhee, and T. Kikuchi (2008), Estimates of surface roughness length in heterogeneous under-ice boundary layers, *J. Geophys. Res.*, *113*, C08030, doi:10.1029/2007JC004550.

Shaw, W. J., T. P. Stanton, M. G. McPhee, J. H. Morison, and D. G. Martinson (2009), Role of the upper ocean in the energy budget of Arctic sea ice during SHEBA, *J. Geophys. Res.*, *114*, C06012, doi:10.1029/2008JC004991.

Shimada, K., E. C Carmack, K. Hatakeyama, and T. Talizawa (2001), Varieties of temperature maximum waters in the western Canada Basin of the Arctic Ocean, *J. Geophys. Res.*, *28*(18), 3441–3444, doi:10.1029/2001GL013168.

Shimada, K., T. Kamoshida, M. Itoh, S. Nishino, E. Carmack, F. McLaughlin, S. Zimmermann, and A. Proshutinsky (2006), Pacific Ocean inflow: Influence on catastrophic reduction of sea ice cover in the Arctic Ocean, *J. Geophys. Res.*, *33*, L08605, doi:10.1029/2005GL025624.

Silverthorne, K. E., and J. M. Toole (2009), Seasonal kinetic energy variability on near-inertial motions, *J. Phys. Oceanogr.*, *39*, 1035–1049, doi:10.1175/2008JPO3920.1.

Skyllingstad, E. D., C. A. Paulson, and W. S. Pegau (2005), Simulation of turbulent exchange processes in summertime leads, *J. Geophys. Res.*, *110*, C05021, doi:10.1029/2004JC002502.

Steele, M., J. Morison, W. Ermold, I. Rigor, M. Ortmeyer, and K. Shimada (2004), Circulation of summer Pacific Halocline water in the Arctic Ocean, *J. Geophys. Res.*, *109*, C02027, doi:10.1029/2003JC002009.

Zhang, J., and M. Steele (2007), Effect of vertical mixing on the Atlantic water layer circulation in the Arctic Ocean, *J. Geophys. Res.*, *112*, C04S04, doi:10.1029/2006JC003732.

R. A. Krishfield, A. Proshutinsky, and J. M. Toole, Woods Hole Oceanographic Institution, Woods Hole, MA 02543, USA.

D. K. Perovich and J. A. Richter-Menge, Cold Regions Research and Engineering Laboratory, Hanover, NH 03755, USA.

M.-L. Timmermans, Yale University, New Haven, CT 06520, USA.